Stratification effects by fine suspended sediment at low, medium, and very high concentrations

J. C. Winterwerp[1,2]

Received 22 April 2005; revised 12 September 2005; accepted 23 January 2006; published 18 May 2006.

[1] This paper describes results of the second part of a study on stratification effects by cohesive and noncohesive sediment. Winterwerp (2001) applied classical stratified flow theory implemented in a one-dimensional vertical numerical model (the 1DV POINT MODEL), showing that sediment-induced stratification effects may occur at already fairly small suspended sediment concentrations (i.e., a few 100 mg/L). We also discussed a basic difference between the behavior of cohesive and noncohesive sediment, which emerges as a result of the large water content of mud flocs. In this paper we elaborate further on the hydrodynamic description of the transport of fine suspended sediment by analyzing field and laboratory observations over a very large range of concentrations. We propose a sediment stability diagram to explain some features of hyperconcentrated flows, such as those observed in the Yellow River. We show that the behavior of hyperconcentrated flows is affected largely by hindered settling effects reducing the energy required to keep the sediment in suspension. The hydrodynamic description of sediment transport is used to predict capacity conditions as a function of a dimensionless stream power, i.e., U^3/hgW_s. This prediction agrees favorably with observations reported in literature covering four orders of magnitude in suspended sediment concentration.

Citation: Winterwerp, J. C. (2006), Stratification effects by fine suspended sediment at low, medium, and very high concentrations, *J. Geophys. Res.*, *111*, C05012, doi:10.1029/2005JC003019.

1. Introduction

[2] *Winterwerp* [2001] discusses stratification effects induced by the interaction between suspensions of fine-grained cohesive and noncohesive sediment with the turbulent flow in estuarine and coastal environments. A concise literature review revealed that this interaction may cause an appreciable modification of the vertical profiles of velocity, vertical eddy viscosity/diffusivity and Reynolds stresses. This interaction was further studied with a one-dimensional vertical numerical model (1DV POINT MODEL), which includes the standard k-ε turbulence model with buoyancy destruction terms. It is derived from the full three-dimensional model DELFT3D [e.g., *Lesser et al.*, 2004] by stripping all horizontal gradients, except for the pressure gradient. Application of this model to the experimental results by *Coleman* [1981, 1986] showed that the measured changes in the velocity profile can be explained entirely by sediment-induced buoyancy effects, as hypothesized by *Vanoni* [1946]. Moreover, it was shown these effects are not limited to the wall region (through a modification of the Von Kármàn constant) or the outer region (through a modification of the defect law parameters) of the boundary layer, but are manifest throughout the entire water column.

[3] It was argued that when the carrying capacity of a turbulent flow laden with noncohesive sediment is exceeded, a new equilibrium at a lower sediment load is formed rapidly as the depositing grains form a rigid bed immediately, at which full turbulence production is possible. This phenomenon is treated in all classical textbooks on sediment transport [*Raudkivi*, 1976; *Graf*, 1977]. However, for cohesive sediment a different picture emerges as the depositing cohesive sediment flocs form a fluid mud layer on the bed because of the floc's high water content. Thus a two-layer fluid system develops in which the lower layer is the denser one. As most of the turbulence is produced in the lower layer by bed friction, significant buoyancy-induced damping of the vertical mixing processes occurs, decreasing the carrying capacity further. This positive feed back results in a catastrophic collapse of the turbulence field and the concentration profile, which was referred to as saturation, and the corresponding concentration is referred to as the saturation concentration c_s. A scaling law for this saturation behavior was derived from classical stratified flow theory. This scaling law was confirmed through a series of numerical experiments with the 1DV POINT MODEL. Also the suspended sediment concentrations observed in the Yellow River were predicted to the right order of magnitude. It was concluded that at already fairly low suspended sediment concentrations appreciable stratification is generated by sediment-induced buoyancy effects, for example, already at a few 100 mg/L.

[4] The concept of saturation is based on the observation that a turbulent shear flow collapses when the flux Richard-

[1]Faculty of Civil Engineering and Geosciences, Delft University of Technology, Delft, Netherlands.
[2]WL|Delft Hydraulics, Delft, Netherlands.

0148-0227/06/2005JC003019$09.00

son number Ri_f (which can be regarded as the ratio between the energy required to mix sediment over the water column and the available kinetic (mixing) energy provided by the flow; hence Ri_f can be regarded as an efficiency parameter for vertical mixing) exceeds a critical value Ri_{cr} [*Turner*, 1973]. Ri_f was further elaborated, assuming a logarithmic velocity profile and local equilibrium between settling and mixing. The effects of hindered settling, as modeled by *Richardson and Zaki* [1954] were included as well. Then, to first order Ri_f can be written as:

$$Ri_f \propto \frac{\rho_s - \rho_w}{\rho_s} \frac{ghW_s c_{gel}}{\rho u_*^3} \phi(1-\phi)^5 \tag{1}$$

in which g is the acceleration of gravity, ρ_w is the density of water, ρ_s is the density of sediment, ρ is the bulk density of the sediment-water mixture, h is the water depth, W_s is the settling velocity of a single sediment particle in still water, u_* is the shear velocity, and ϕ is the volumetric sediment concentration, defined as $\phi = c/c_{gel}$, where c is the mass concentration of the suspended sediment and c_{gel} its gelling concentration, i.e., the concentration at which the suspension forms a space-filling network. The factor between parentheses in (1) accounts for the effects of hindered settling according to *Richardson and Zaki* [1954]. Intuitively it is anticipated that capacity conditions are met when Ri_f becomes critical over the entire water depth. This assumption is sustained by the analysis of data in the Amazon mouth by *Trowbridge and Kineke* [1994], showing a more or less constant Richardson number at capacity conditions. Thus a relation for the saturation concentration C_s, which is the depth-averaged value of the local saturation concentration c_s was derived [see *Winterwerp*, 2001]:

$$C_s \equiv \frac{1}{h}\int_0^h c_s \mathrm{d}z = K_s \frac{\rho}{\Delta} \frac{U^3}{ghw_s} \tag{2}$$

where K_s is a proportionality factor ($K_s\rho/\Delta = \mathrm{O}\{0.1-1\}$ [e.g., *Winterwerp and Van Kesteren*, 2004], Δ is the relative sediment excess density ($\Delta = (\rho_s - \rho_w)/\rho_s$), U is the depth-averaged flow velocity and w_s is the effective settling velocity, including the effects of hindered settling. Hence UC_s is a measure for the sediment transport capacity of the turbulent flow. In fact, the scaling law for saturation (2) is almost identical to *Bagnold*'s [1966] sediment transport formula (see also section 4).

[5] Relation (1) is plotted in the stability diagram of Figure 1. One can distinguish between subsaturated and supersaturated conditions, i.e., when $Ri_f < Ri_{cr}$ and $Ri_f > Ri_{cr}$, respectively. In the left-hand side of the diagram, at very small concentrations (sediment load), sediment-induced buoyancy effects are not important. At larger concentrations, but still in the subsaturated regime, sediment-induced buoyancy effects become important affecting vertical mixing, hence the vertical concentration and velocity profiles. When the concentration increases further, given a particular flow field, capacity conditions are exceeded and the suspension gets saturated, followed by a collapse of the turbulence field.

[6] At much larger concentrations, subsaturated conditions are reestablished, as the vertical sediment flux decreases because of hindered settling effects. This regime is referred to as the hyperconcentrated regime. Thus four regimes are identified in Figure 1: (1) supersaturated conditions ($Ri_f > Ri_{cr}$); that is, the turbulent flow is unstable and cannot carry the sediment load available; (2a) subsaturated, low-concentration suspensions at small Ri_f numbers without sediment-fluid interaction; the amount of sediment carried by the flow is far below its capacity; (2b) subsaturated, high-concentration suspensions at large Ri_f numbers, but below critical, with pronounced sediment-fluid interactions; the amount of sediment carried by the flow is at, or near its capacity, and (2c) subsaturated, hyperconcentration suspensions at large Ri_f numbers, but below critical, with pronounced sediment-fluid interactions.

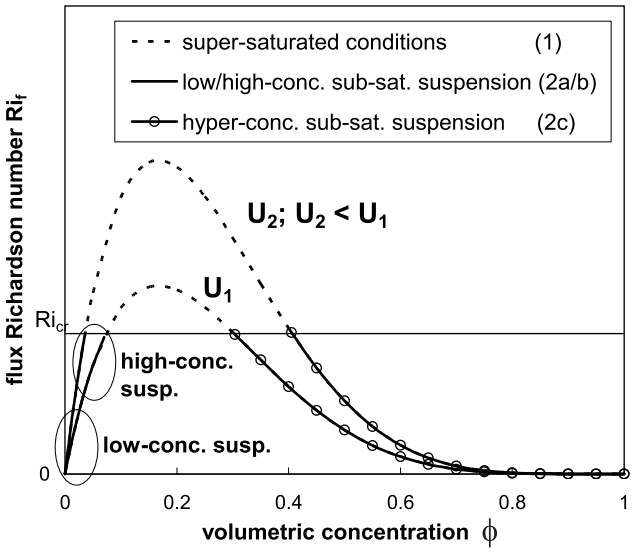

Figure 1. Stability diagram for sediment-laden flow, showing stability curves for two different flow velocities U_1 and U_2. The numbers in parentheses refer to the regimes described in the text.

[7] This diagram can be used to analyze the behavior of sediment-laden flow in the case that either the amount of suspended sediment and/or the flow velocity increases or decreases. In the subsaturated, low-concentrated regime (2a), a sufficient increase in sediment concentration (ϕ) (e.g., sediment load) and/or a decrease in flow velocity (from U_1 to U_2) will induce sediment-induced stratification effects, shifting the behavior of the suspension from regime 2a to 2b. A further increase in sediment concentration and/or decrease in flow velocity may result in a collapse of the concentration profile and of the turbulent flow field (regime 1).

[8] The behavior of sediment-laden flows at hyperconcentrated, subsaturated conditions (2c) is completely different. In this region, an increase in sediment load (ϕ) results in a stabilization of the flow, as Ri_f decreases with ϕ. As moreover the suspension's density increases with ϕ, the driving forces on the sediment-laden flow increase. This explains why turbidity currents, which can be regarded as a manifestation of this regime, can be so persistent and devastating. We will see that this is also the case for the Yellow River and its tributaries in the hyperconcentrated regime.

Table 1. Parameter Settings 1DV POINT MODEL for *Cellino and Graf*'s [1999] Experiments

Parameter		CW	SAT
Water depth	h	0.12 m	0.12 m
Mean flow velocity	U	0.726 m/s	0.853 m/s
Bed roughness	k_s	1.2 mm	1.2 mm
Shear velocity experimental	u_*	0.045 m/s	0.045 m/s
Prandtl-Schmidt number	σ_T	0.7	0.7, 2.0
Shear velocity 1DV model	u_*	0.045 m/s	0.051 m/s, 0.049 m/s
Water density	ρ_w	1000 kg/m^3	1000 kg/m^3
Kinematic viscosity	ν	10^{-6} m^2/s	10^{-6} m^2/s
Sediment density	ρ_s	2650 kg/m^3	2650 kg/m^3
Initial sediment concentration	C_0	0	3.9 kg/m^3
Median grain size	D_{50}	135 μm	135 μm
Hindered settling		yes	yes
Water-bed exchange		no	no
Number of layers		100	100
Time step	Δt	0.05 s	0.05 s

[9] A decrease in flow velocity (from U_1 to U_2) in this region, as a result of for instance channel divergence and/or decreasing river flow, may also have a devastating effect. As the capacity conditions scale with U^3, and the (volumetric) sediment concentration is large, a decrease in flow velocity may lead to "freezing" of the turbulent suspension. This disturbance propagates upstream, blocking the flow rapidly. This phenomenon is known from slurry transport through pipes and has been observed in tributaries of the Yellow River as well [*Xu*, 1999a, 2003].

[10] In this paper we elaborate further on this hydrodynamic approach of sediment-laden flow and present some examples of application, covering a wide range of conditions with concentrations varying between a few 100 mg/L to about 1,000 g/L. First, in section 2 we discuss the behavior of sediment-laden flow in the lower-concentration regime, and in section 3 in its higher regime. Section 4 contains a synthesis in which the entire concentration regime is integrated. This paper is finalized in section 5 with a discussion on the applicability of the hydrodynamic approach to analyze the behavior of sediment-laden flow.

2. Applications in the Lower-Concentration Regime

[11] In this section we analyze the behavior of sediment-laden flow in the lower-concentration regime. First, we discuss results from laboratory experiments, where after more natural systems are treated.

[12] *Cellino and Graf* [1999] measured the mean and fluctuating velocity components and suspended sediment concentration acoustically at a frequency of 39 and 16 Hz, respectively, in a flow laden with noncohesive sediment through a 16.8 m long and 0.6 m wide tilting flume. The flow depth was kept constant at 0.12 m and the flow velocity was varied between 0.73 and 0.85 m/s. Experiments were carried out in clear water and at varying sediment loads until capacity conditions. The median diameter of the suspended sediment amounted to 135 μm, whereas 4.8 mm sand grains were glued to the flume bottom. Only in the case of capacity conditions (see below) fine sediment deposited on the bottom. Cellino and Graf were able to measure vertical profiles of the mean flow velocity and suspended sediment concentration profiles, and of the turbulent kinetic energy, Reynolds stress and eddy viscosity as a function of the sediment load.

[13] The results of these benchmark experiments have been used for a further analysis of the interaction of suspended sediment and the turbulent flow field, using the 1DV POINT MODEL. In particular, the experimental series CW and SAT at respectively clear water and capacity conditions have been analyzed (see Table 1).

[14] The equivalent sand roughness height k_s for clear water was set to *Cellino and Graf*'s [1999] experimental value; for saturated conditions, the same value was used, assuming that the 1DV POINT MODEL predicts the effects on bed roughness of the larger flow velocity and suspended sediment load properly. The computed vertical profiles of flow velocity, relative suspended sediment concentration and relative eddy viscosity (see Table 1 for parameter settings) are compared with the experimental data in Figures 2–4. It is shown that the 1DV POINT MODEL predicts that

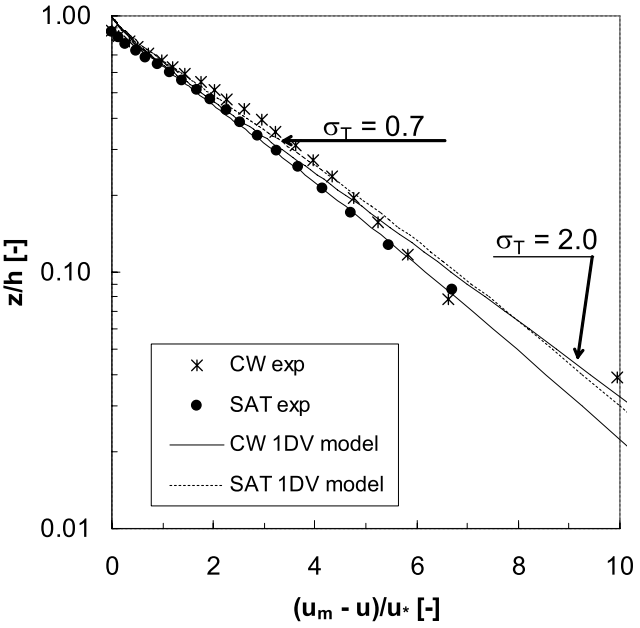

Figure 2. Measured and computed vertical velocity profiles in defect law form.

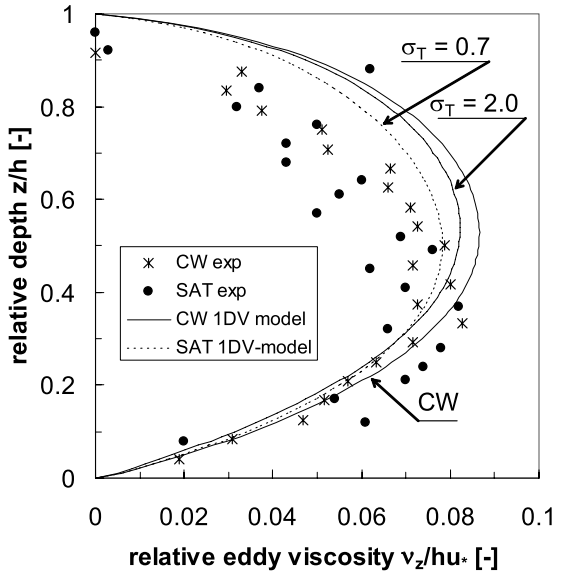

Figure 3. Measured and computed relative vertical eddy viscosity profile.

the buoyancy effects result in a slight decrease in the slope of the velocity profile in defect form, contrary to the observations. However, it is noted that *Graf and Cellino* [2002] present other series of experimental results, which show the computed trend. This computed trend also agrees with the data by *Coleman* [1981, 1986; e.g., *Winterwerp*, 2001]. At this moment we have no explanation for this anomalous behavior.

[15] The computations show a small, but systematic decrease in eddy viscosity with increasing sediment concentration (Figure 3). This is more or less in agreement with the observations, though in absolute terms, the agreement between computed and measured values is not perfect. In particular, the data appear to be more skewed than the computational profile, which is still more or less parabolic. The agreement between the computed and observed vertical concentration profile (Figure 4) is reasonable, though not perfect either, which of course is due to the differences between computed and observed flow parameters. It is noted that *Cellino and Graf* [1999] found capacity conditions at their SAT conditions, i.e., at $C_0 = 3.9$ g/L (where C_0 is the initial depth-averaged concentration, denoted as C_s for saturation conditions). However, the 1DV POINT MODEL predicts saturation, i.e., capacity conditions at much larger values, i.e., of the order of $C_s = 15$ g/L.

[16] In the 1DV POINT MODEL, the standard k-ε turbulence model is used, with standard coefficients. In particular, the turbulent Prandtl-Schmidt number is kept constant at $\sigma_T = 0.7$ (where $\sigma_T = \nu_z/\Gamma_z$, with Γ_z = eddy diffusivity). However, the experimental data suggest a considerable increase in σ_T with increasing C_0. For instance, for the SAT experiments, *Cellino and Graf* [1999] found a depth-averaged value of $\sigma_T = 2$. Therefore the 1DV POINT MODEL was run for $\sigma_T = 2$ as well, the results of which are also presented in Figures 2–4. It is shown that the effect on vertical profiles of velocity and eddy viscosity is not large. The effect on the eddy diffusivity, however is large, of course (results not shown), and also a pronounced effect on the concentration profile is shown – in fact the agreement between predictions and observations has improved considerably. With this higher Prandtl-Schmidt number, saturation (capacity conditions) is computed at about $C_s \approx 5$ g/L, i.e., close to the value reported by *Cellino and Graf* [1999].

[17] In section 4 the effect of the Prandtl-Schmidt number on the capacity conditions and its rationale is further elaborated. Here we conclude again that the behavior of flows laden with fine sediment can be analyzed properly with the hydrodynamic approach implemented in the 1DV POINT MODEL.

[18] A natural example of a sediment-driven gravity flow at low/moderate concentrations can be seen on the aerial photograph in Figure 5 of the Port of Zeebrugge situated along the Belgium coast. This photograph was taken on 18 October 1993 between 14:00 and 15:00 hrs, i.e., 1 to 2 hours before high water; the tidal range that day amounted to about 5.2 m. The flow in this phase of the tide is north (to the left in Figure 5), with an estimated velocity of about 1 m/s [*Royal Navy*, 1986]. The hydro-sedimentological conditions at the North Sea are in the lower-concentration regime (2a), i.e., in the left part of the stability diagram of Figure 1.

[19] The water temperature is not known. However, the air temperature in the month prior to the photograph varied between 10° and 20°C, decreasing to 3°–10°C in the last week before the photo. This implies that if temperature differences between harbor basin and surrounding North Sea would exist, the basin most likely would be the cooler of the two.

[20] From this information, the following picture can be deduced. The tide is still rising, hence there should be a net inflow of water through the harbor entrance. As the surface area of the basin is about 7 km^2, and the cross section of the entrance measures about 650 × 15 m^2, the mean tide-induced velocity of the inflow through the entrance is about 0.1 m/s at this phase of the tide. However, at the water surface we observe a front with a distinct outflow. This is

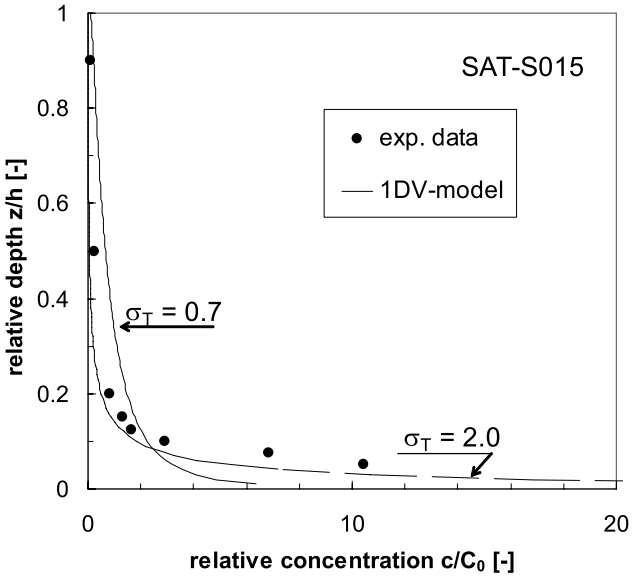

Figure 4. Measured and computed relative vertical suspended sediment concentration profile.

Figure 5. Aerial photograph of Port of Zeebrugge located in the Belgium coastal zone of the North Sea. The surface water within the harbor basin is almost clear, whereas the ambient water is highly turbid. The front of outflowing clear water is indicated with an arrow.

only possible if an exchange flow exists in the harbor mouth. This exchange flow is generated by density currents, induced by the horizontal gradients in suspended sediment concentration across the harbor entrance (note that no fresh or warm water is released in the basin and possible temperature-induced density gradients would generate outflow at the water surface, as reasoned above).

[21] The outflow at the water surface should have a velocity of about 0.1 m/s to just counterbalance the tidal filling effect. Let us assume double critical flow conditions in the entrance, as observed in classical lock exchange experiments, and zero sediment concentration in the water column within the harbor. Then the velocity of such exchange flows can be computed from $u \approx 0.5\sqrt{\Delta\rho g h/\rho}$ [e.g., *Barr*, 1967], in which $\Delta\rho$ is the density difference between the water in the basin and at sea and h is the depth of the entrance. Using the estimated velocity of about 0.1 m/s, this yields a suspended sediment concentration at sea of about 0.4 g/L, which is in the range of the observed values of several hundreds of mg/L [*Bastin et al.*, 1984]. Therefore it is concluded that, at the time the photograph was taken, a two-layered system existed in the harbor entrance with some outflow in the upper layer and a significant ($U >$ 0.2 m/s) inflow of sediment-laden water in the lower layer. The sediment in the lower layer spreads more or less evenly throughout the basin, settles and contributes to the large volumes of sediment that have to be dredged annually to safeguard navigation.

[22] Apparently, suspensions at relatively low concentrations may generate considerable density currents, as anticipated from our analysis of the stability diagram of Figure 1: low-concentrated subsaturated sediment-laden flow may develop into high-concentration flows when the flow velocity decreases sufficiently. Sediment-induced stratification effects start to play a role, and even saturation may occur if the flow velocity decreases enough (i.e., the suspension evolves from regime 2a to 2b to 1, Figure 1). This is what is happening to the suspension on the North Sea in Figure 5, when it enters the enclosed basin of the Port of Zeebrugge.

[23] This behavior is further illustrated through a simulation of the sediment transport in the Maasmond area, i.e., the entrance to the Port of Rotterdam, Netherlands (see Figure 6a) with a full three-dimensional hydrodynamic and sediment transport model (i.e., the DELFT3D system). The computations were carried out with and without sediment-fluid interaction (i.e., sediment-induced buoyancy effects in the turbulence model, hindered settling and baroclinic pressure effects in the momentum equations; see *Winterwerp and van Kessel* [2003] for details). Results of tide-averaged suspended sediment concentrations in the lower layer of the computational grid are presented in Figure 7.

[24] The large differences in suspended sediment concentration result in large differences in computed sediment fluxes (hence siltation rates) in the Maasmond area, as depicted in Table 2. The cross sections at which the fluxes have been computed are indicated in Figure 7 (right). This table shows that the net calculated flux over a tidal cycle through cross section 1, Maasmond mouth, almost triples when sediment-induced buoyancy effects are taken into account. This is the result of an increase in both the gross import and gross export, though the increase in import is the larger of the two. The major differences between the two simulations are found in the lower layers: in the case of inclusion of sediment-fluid interaction, the concentration profile becomes highly stratified, forming a layer of fluid mud in the harbor basins.

[25] These computations have been performed with an inflow concentration at the model boundaries of 100 mg/L. This is a characteristic value for windy winter conditions. Table 2 implies that after a storm siltation rates of 200,000 to 300,000 m^3 (assuming deposit densities of about 1200 to 1300 kg/m^3) can be expected in the port area, values which indeed have been observed [*Verlaan and Spanhoff*, 2000].

[26] For typical summer conditions, with a boundary concentration of 10 to 50 mg/L, the effect of sediment-fluid interaction on the sediment fluxes was computed at 10% only. As the sediment-fluid interactions are highly nonlinear, it may be expected that the increase in sediment flux would increase rapidly when the suspended sediment concentration at sea increases to several 100 mg/L, values which have been measured in the Dutch coast under long-lasting storm conditions.

3. Applications in the Hyperconcentration Regime

[27] In this section we elaborate on the conditions in the right-hand part of Figure 1, i.e., the hyperconcentration flow regime (2c). An obvious candidate for further studies is the Yellow River, though it is anticipated that many turbidity currents, debris flows and slurries in pipelines fall within this category as well.

[28] The annual mean river flow in the Lower Yellow River decreased from about 1630 m^3/s to about 580 m^3/s

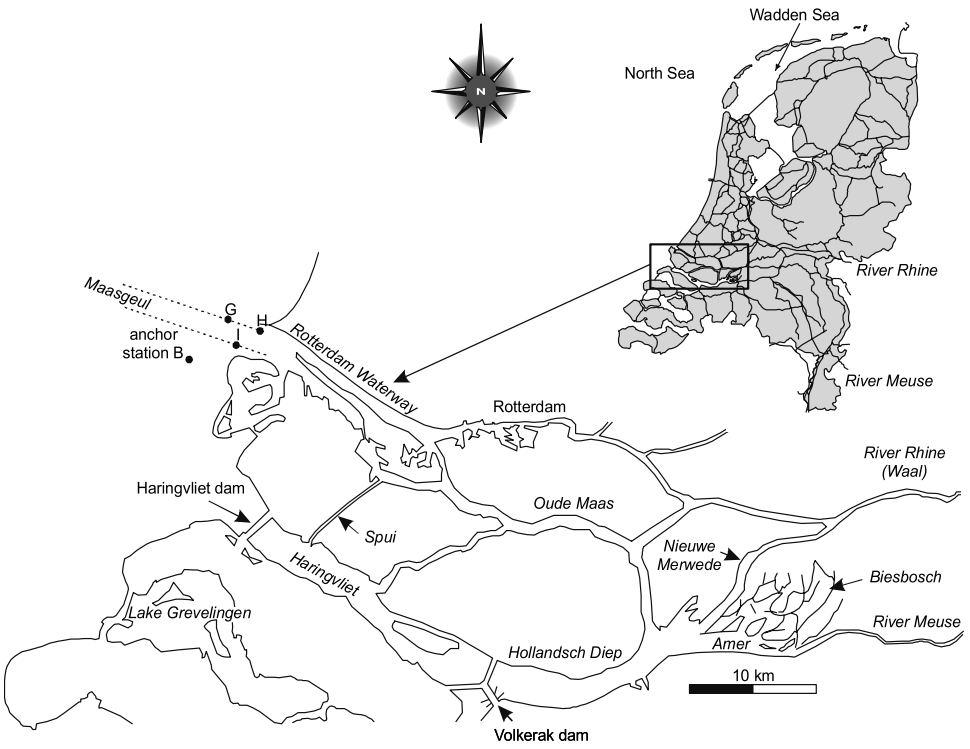

Figure 6. Location of Maasmond area in Netherlands.

during the last decades. Peak flows are twice as high in August and low runoff (40% of mean values) occurs in December/January [e.g., *Liu et al.*, 2003]. Under high-flow conditions, the river is heavily laden with very fine sediment (loess) originating from the Loess Plateau in the middle reach of the river, to the extent that hyperconcentration conditions may occur. The mean annual sediment load at Samenxia has reduced from $1.6 \cdot 10^9$ ton to about $0.8 \cdot 10^9$ ton, yielding a decrease in annual mean suspended sediment concentration from about 80 g/L to about 38 g/L, with maximum values up to 911 g/L [*Wang and Xu*, 1999; *Xu*, 1999a]. In some tributaries, concentrations up to 1500 g/L have been reported [e.g., *Chien and Wan*, 1999].

[29] We apply the 1DV POINT MODEL in the same way as was done by *Winterwerp* [2001]; that is, the initially homogeneously distributed sediment concentration in open channel flow at uniform conditions is altered in small steps until saturation occurs, starting from subsaturated conditions. This time, however, we decrease the initial concentration to obtain saturation conditions, anticipating on the stability diagram of Figure 1.

[30] The evolution with time of the vertical concentration profile and the hydrodynamic parameters is computed and the concentration profiles are visualized in the form of isolutals (i.e., lines of constant sediment concentration). The initial concentration is changed in small steps until the concentration and flow profile collapse. The concentration just prior to this collapse is referred to as the saturation concentration, or capacity load.

[31] The various model settings are summarized in Table 3. The hypothetical channel has a depth of 5 m, and the mean flow velocity is set at 1 m/s. These values are more or less characteristic for the Yellow River. The median grain size is set at 30 μm and D_{90} at 100 μm, so that the

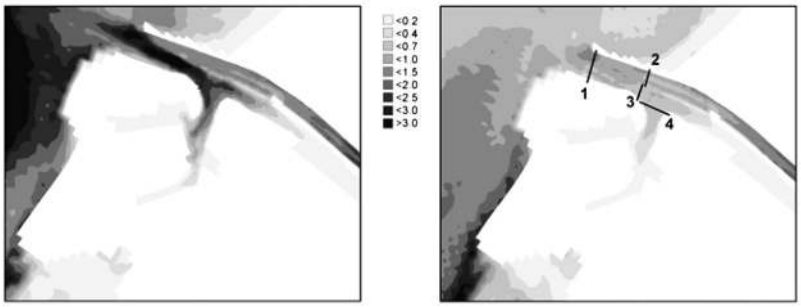

Figure 7. Tide-averaged sediment concentration [g/L] near the bed in the entrance to the Port of Rotterdam computed (left) with and (right) without sediment-fluid interactions.

Table 2. Mean Water and Sediment Fluxes for Rotterdam Harbor Area[a]

		Sediment Flux, kg/s			Water Flux, m^3/s		
Inter Act.	Cross Section	Tidal Net	Gross Import	Gross Export	Tidal Net	Max. Ebb	Max. Flood
No	1. Maasmond	325	719	−395	−1263	−12886	10298
Yes	1. Maasmond	884	1503	−620	−1264	−12929	10575
No	2. R'dam Waterway	50	365	−315	−1292	−8959	5476
Yes	2. R'dam Waterway	76	466	−390	−1304	−9067	5490
No	3. Calandkanaal	263	307	−44	0	−3518	5452
Yes	3. Calandkanaal	792	828	−35	0	−3457	5470
No	4. Beerkanaal	126	131	−5	0	−2095	1505
Yes	4. Beerkanaal	404	413	−8	0	−2119	1481

[a]See Figure 7 for definition cross sections.

roughness height k_s amounts to 0.3 mm [e.g., *Wan and Wang*, 1994; *Xu*, 1999a]. All sediment remains in the computational domain; that is, no erosion from or deposition on the riverbed occurs.

[32] The results presented in Figures 8a–8c (note different concentration scales) are typical for Yellow River conditions. Figure 8a and b show the isolutals for an initial depth-averaged concentration of C_0 = 975 and C_0 = 965 g/L, respectively. Saturation now occurs when the sediment concentration is decreased, as anticipated in section 1. Note that the equivalent saturation concentration in the high-concentration regime (2b) amounts to C_0 = 2.4 g/L, the results of which are not shown here.

[33] The effect of the buoyancy destruction term in the k-ε model is illustrated in Figure 8c, showing computational results without coupling (i.e., no sediment-induced buoyancy term in the k-ε equation), but with hindered settling effects, revealing an almost homogeneous concentration profile (compare with Figure 8b).

[34] The effect of concentration and buoyancy is further illustrated in Figures 9 and 10, showing the computed vertical velocity and eddy viscosity profiles. In the uncoupled case, a common logarithmic velocity profile and parabolic eddy viscosity profile are computed. For near-saturation conditions (coupled, C_0 = 975 g/L), the eddy viscosity decreases rapidly, and a stratified flow system occurs in which the near-surface flow appears to accelerate to large velocities. In the saturated case, the viscosity becomes virtually zero, and the velocity profile becomes parabolic as for laminar flow [e.g., *Chien and Wan*, 1999]. It is noted that the standard k-ε model is no longer valid for these conditions, as low-Reynolds, non-Newtonian and soil mechanical effects start to play a role. Yet, the laminar flow profile obtained seems reasonable and agrees with observations [e.g., *Chien and Wan*, 1999].

[35] In comparison to the high-concentration regime [e.g., *Winterwerp*, 2001] (e.g., section 2), the timescale of collapse is very large, i.e., of the order of months. This is due, of course, to the very small settling velocity, reduced by hindered settling to about 0.04%–1% of the nonhindered settling value (i.e., $(0.03–9).10^{-6}$ m/s). Hence such suspensions can be very persistent. Moreover, these suspensions become more stable, as said, when they pick up sediment through erosion, because if the sediment concentration increases, the suspension moves away from the saturation point in the stability diagram, and upon entraining more sediment, the suspension's driving force increases, accelerating the current. It is noted that the capacity of a hyperconcentration suspension to erode its bed is not as large as one would expect because of two effects: (1) the permeability of the loess soil is very small, so that water can replace eroding sediment particles only at a slow rate, and (2) erosion of the underlying bed is retarded because water cannot flow easily from the suspension into the bed. This phenomenon is referred to as hindered erosion. The erosion rate decreases by a factor $(1 - n - \phi)/(1 - n)$, where n is the bed's porosity [e.g., *Winterwerp et al.*, 1992].

[36] However, erosion of the riverbank is easier because of breaching and massive failure of the banks. Large boulders are easily suspended by the silt-laden flow, with excess bulk densities of several hundred kg/m^3.

[37] We conclude that our hydrodynamic approach can explain a number of features typical for the Yellow River. However, a full understanding and proper modeling will

Table 3. Reference Parameter Settings in 1DV POINT MODEL

Parameter		Value	Remarks
Water depth	h	5 m	
Mean flow velocity	U	1 m/s	flow rate constant
Bed roughness	k_s	$3 \times D_{90}$	hydraulically rough
Water density	ρ_w	1000 kg/m^3	
Sediment density	ρ_s	2700 kg/m^3	
Gelling concentration	c_{gel}	1600 kg/m^3	
Initial sediment concentration	C_0	variable	homogeneous profile
Median grain size	D_{50}	30 μm	
"Coarse" grain size	D_{90}	100 μm	
Hindered settling		yes	*Richardson and Zaki* [1954]
Water-bed exchange		no	
Prandtl-Schmidt number	σ_T	0.7	
Number of layers		100	equidistant
Time step	Δt	1 min	

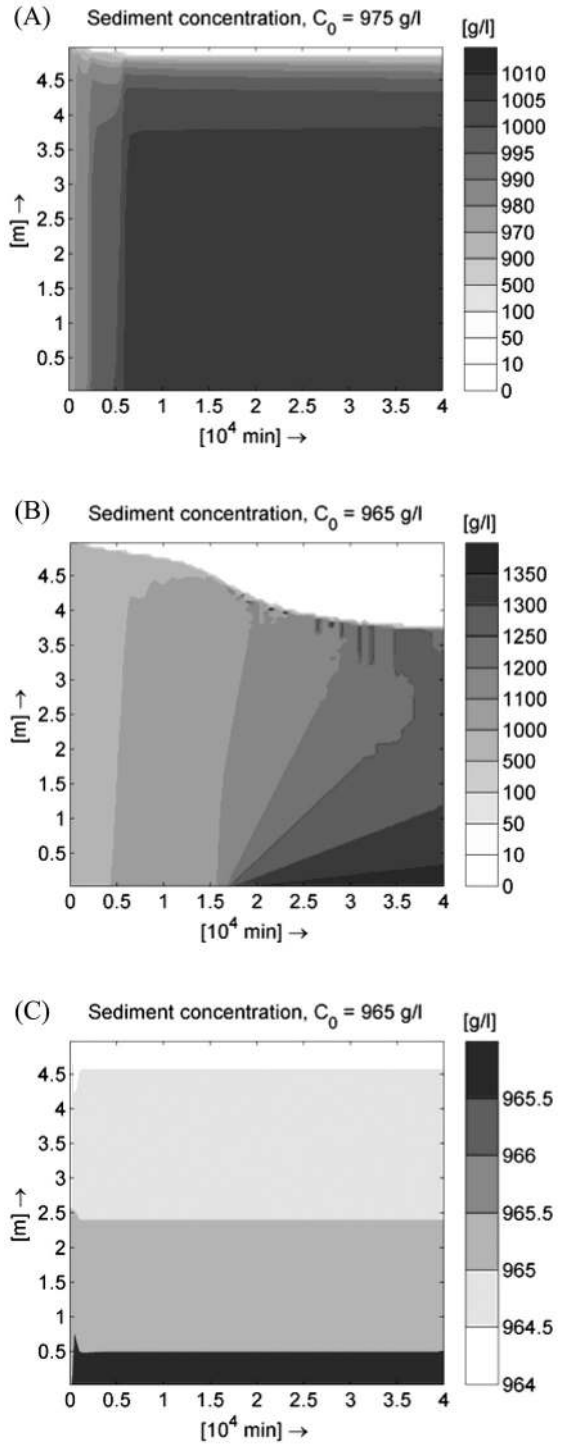

Figure 8. Table 3 model settings, hyperconcentrated regime: (a) isolutals for C_0 = 975 g/L, (b) isolutals for C_0 = 965 g/L (note different scales), and (c) isolutals for C_0 = 965 g/L; same as Figure 8b, but no sediment-fluid interaction (note different scales).

require much more research. In particular, the following issues have to be addressed: (1) The effect of non-Newtonian behavior of the suspension, to account for the effects of very high suspended sediment concentrations on the stress-strain relations, in particular near the bed

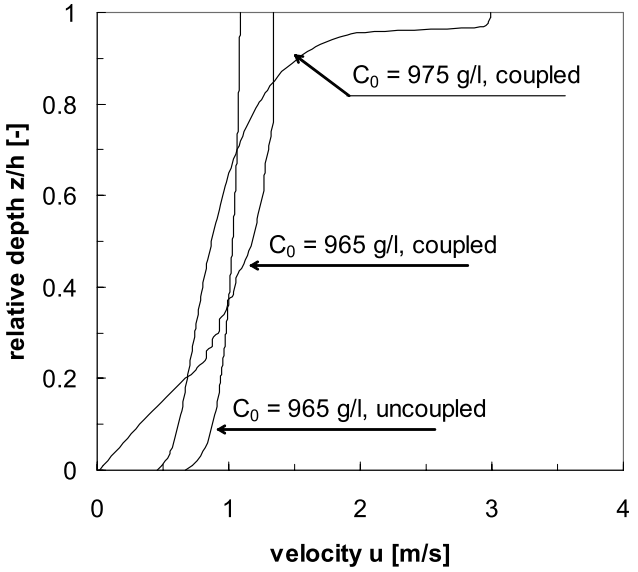

Figure 9. Table 3 model settings, hyperconcentrated regime: vertical velocity profiles.

(amongst these are the effects of grain-grain interactions.); (2) soil mechanical influence on the bed stability to account properly for water-bed exchange processes and bank instability; and (3) interaction of the flow with its bed, for example, the highly dynamic morphological behavior of the river, which may result in changes in thalweg and river cross sections, even within one flood. These items are subject of further research.

4. Integration of the Concentration Regimes

[38] Sections 2 and 3 analyze simulations with the 1DV POINT MODEL for the high-concentrated and hyperconcentrated, subsaturated regimes. The results follow the behavior of the stability diagram of Figure 1. This implies

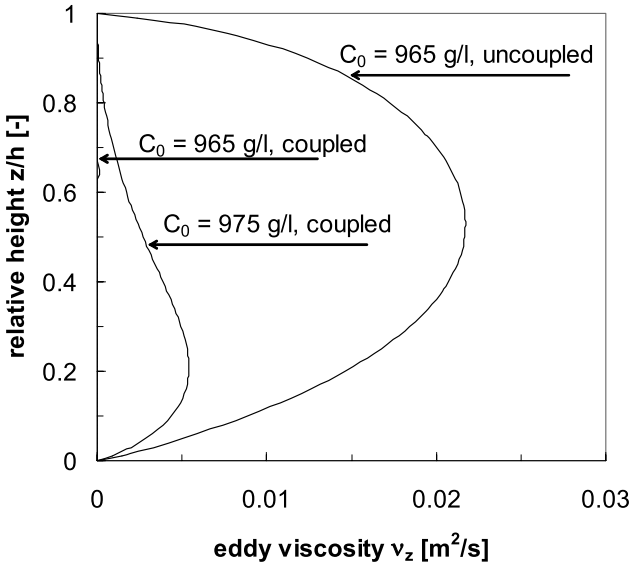

Figure 10. Table 3 model settings, hyperconcentrated regime: vertical viscosity profiles.

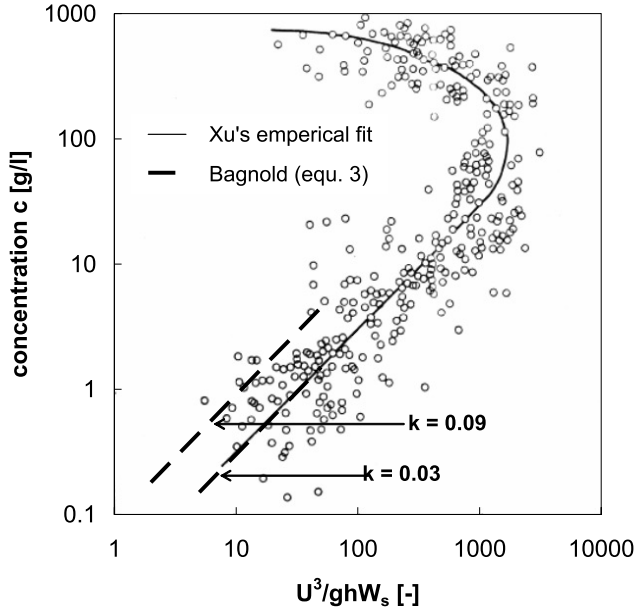

Figure 11. Data on depth-averaged suspended sediment concentration by *Xu* [1999b] compared for low concentrations with Bagnold's transport formula (3); $C = 60\ \mathrm{m}^{1/2}/\mathrm{s}$.

that at high-concentration and hyperconcentration conditions the same sediment-water interaction processes play a role, though at different scale. However, in the case of hyperconcentration conditions, water-bed exchange processes may be affected by mass erosion and hindered erosion processes. This is subject of further studies and beyond the scope of the current paper.

[39] Figure 11 presents data by *Xu* [1999b], based on observations from natural rivers, mainly the Yellow River and its tributaries, irrigation channels and laboratory flumes. These data comprise sediment in the range from silt to fine sand, though no details are given by Xu, and cover almost four orders of magnitude in suspended sediment concentration. Also *Bagnold*'s [1966] transport formula is plotted in this graph, which is given by:

$$q_s \equiv \int_h uc\mathrm{d}z = \frac{e_s(1-e_b)\rho_s\tau_b U^2}{(\rho_s-\rho_w)W_s} \tag{3}$$

Here q_s is the specific suspended load transport, e_b and e_s are efficiency factors ($0.1 < e_b < 0.2$ and $0.01 < e_s < 0.02$) and τ_b is the bed shear stress. If we assume a Chézy coefficient $C = 60\ \mathrm{m}^{1/2}/\mathrm{s}$, equation (3) yields $C_s \approx kU^3/ghW_s$, in which k varies between ~0.03 and ~0.09 as a result of the variations in efficiencies e_b and e_s (see Figure 11).

[40] Bagnold's transport formula is known to describe the transport of fine suspended sediment in riverine systems fairly accurately. As the envelope of this formula, given by the range in k values, matches the lower left data given by *Xu* [1999b] in Figure 11 quite well, we may conclude that Xu's data are in agreement with other river data. It is noted that in particular for $k = 0.03$, Bagnold's formula fits Xu's low-concentration data very well.

[41] Next, equation (2) is applied and compared with the data by *Xu* [1999b]. For this purpose, the 1DV POINT MODEL is run to establish K_s. This has been done for the conditions given in Table 3, but in the high-concentration regime (regime 2b), resulting in a saturation concentration $C_s = 2.4$ g/L, yielding $K_s = 5.9 \cdot 10^{-5}$. This value has been substituted into equation (2), together with the effects of hindered settling according to *Richardson and Zaki* [1954], in which the gelling concentration was set at $c_{gel} = 1600\ \mathrm{kg/m^3}$. The saturation concentration C_s, computed with equation (2) and said K_s, is plotted against the dimensionless stream power U^3/ghW_s in Figure 12, together with Xu's data. The agreement between the theoretical curve of equation (2) and the data is remarkable, though the actual saturation concentration (capacity) is overpredicted a bit, in particular at the lower concentrations.

[42] In a next numerical experiment, the Prandtl-Schmidt number in the 1DV POINT MODEL is increased to $\sigma_T = 2.0$, as suggested by the data from *Cellino and Graf* [1999] and discussed in section 2. In this case a saturation concentration of $C_s = 0.9$ g/L for Table 3, regime 2b conditions is found as shown in Figures 13a and 13b. The 1DV model then yields $K_s = 2.2 \cdot 10^{-5}$ which value is used to plot equation (2) again in Figure 12. The agreement at lower concentrations is now excellent, but in the hindered settling regime (supersaturation regime), the agreement becomes a little less. Note that an increase in σ_T can be interpreted as a decrease in mixing efficiency, as the flow's carrying capacity decreases because of a decrease in vertical mixing, which in this case corresponds to a decrease in Ri_{cr} by about 2/3.

5. Discussion and Conclusions

[43] We have shown that the behavior of sediment-laden flow in both the high-concentrated and hyperconcentrated

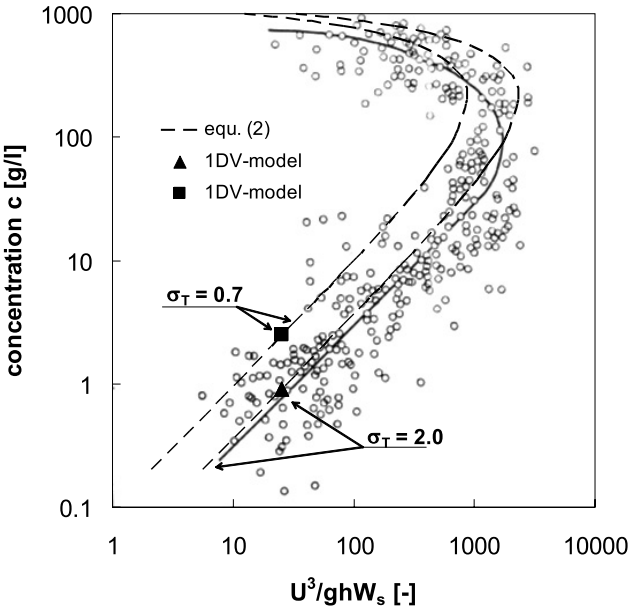

Figure 12. Capacity conditions represented by the maximal depth-averaged concentration that can be maintained by the flow, computed with equation (2) and compared with data by *Xu* [1999b].

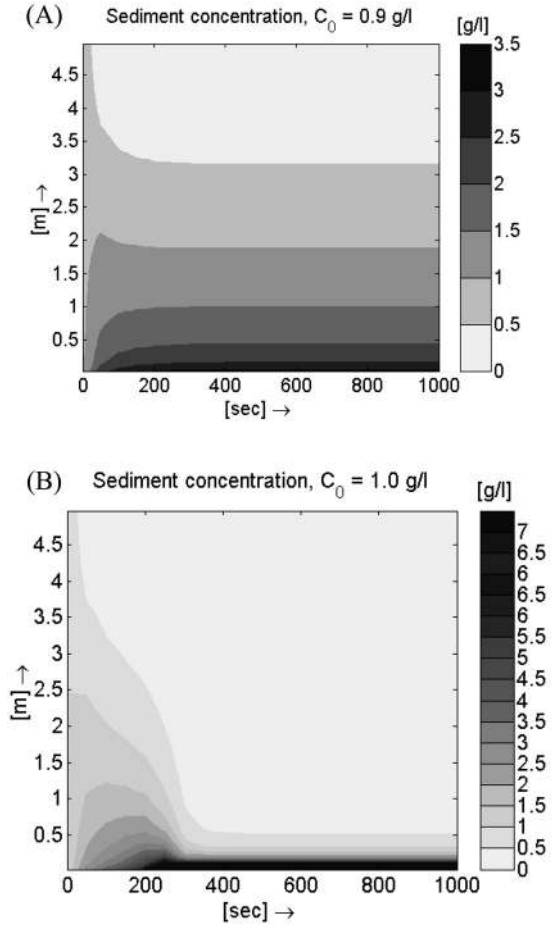

Figure 13. Table 3 model settings, high-concentration regime: (a) isolutals for C_0 = 0.9 g/L and (b) isolutals for C_0 = 1.0 g/L (note different scales).

regimes is governed by the same stratification effects, and that these effects can be analyzed and quantified with classical stratified flow theory. The difference of behavior in these regimes is caused by hindered settling effects which reduce the energy required to keep the sediment in suspension with increasing concentration.

[44] Sediment-laden flows in the high-concentrated and hyperconcentrated regime have been simulated with a standard hydrodynamic model, in which the standard k-ε turbulence closure model with buoyancy destruction is implemented. The results of these simulations appeared to be sensitive to the value of the turbulent Prandtl-Schmidt number (also known as the "β coefficient" in sediment transport literature). It is noted that there exists quite some controversy on the value of σ_T, a concise summary of which has recently been presented by *Nielsen and Teakle* [2004]. They conclude that for fine sediment over a flat bed σ_T seems to increase with respect to neutral conditions, whereas for coarser sediment over beds with bed forms, σ_T is always observed to decrease with increasing grain size; that is, the efficiency of mixing would increase. The latter response is elaborated by *Nielsen and Teakle* [2004] through an expansion of the mixing length theory. Also *Nezu and Azuma* [2004] found a decrease in σ_T with increasing grain size, but they attributed this to grain-grain interactions.

[45] However, in the present study we focus on suspensions of fine sediment that obey single-phase descriptions. In that case, an increase in Prandtl-Schmidt number with increasing sediment concentration is in agreement with the observations in the preceding paragraph. This is also plausible from a physical point of view. It has been known for a long time that in stratified flows, the turbulent exchange of matter is more damped than that of momentum [e.g., *Turner*, 1973], as internal waves transport momentum, but not matter. Moreover, as the sediment particles grow in size, they are less able to follow the turbulent water movement [*Uittenbogaard*, 1995a, 1995b; *Muste and Patel*, 1997]. This would imply that the Prandtl-Schmidt number should at least become a function of the local flux Richardson number Ri_f and the Rouse number β (= $W_s/\kappa u_*$), hence cannot be kept constant.

[46] It is further noted, that, in particular for coarser material, the diffusion concept (and the k-ε model) may fail to be valid. Moreover, we have not accounted for a variety of processes, such as the energy required to mobilize sediment from the bed, the energy loss by grain-grain interactions, the changes in effective bed friction (the horizontal axis of Figure 12 should preferably contain the shear velocity instead of a depth-mean velocity), etc. Finally, it is noted that for tidal flow conditions slightly different scaling laws can be derived [*Winterwerp*, 2002].

[47] In spite of all these limitations and nuances, the results of the hydrodynamic approach of sediment transport are promising. Even in situations where saturation, as proposed in this study, may not occur actually, or only under restricted conditions [e.g., *Winterwerp*, 2001], there is ample evidence that the behavior of sediment-laden flow may be affected strongly by buoyancy effects, even at fairly low suspended sediment concentrations, as low as the order of 100 mg/L. The hydrodynamic approach proposed herein allows a framework to classify the behavior of sediment-laden flow and explain its behavior over a wide range of conditions, not only in natural systems, but most likely also in engineered systems, such as slurries through pipelines. In the latter case, the effects of turbulence production at the pipe wall have to be accounted for. Note that basically only four processes have to be accounted for to model the effects described in this paper: (1) augmented bulk density by suspended sediment in the equation of state, (2) a sediment-induced buoyancy destruction term in the turbulence closure equation, (3) hindered settling in the sediment balance equation, and (4) a baroclinic pressure contribution in the horizontal momentum equation. A next step to improve the physical description of hyperconcentrated flow and its modeling is to account for low Reynolds effects, non-Newtonian effects and the inclusion of soil mechanical theory to allow an implicit description of the processes at the water-bed interface. This is subject of ongoing research.

Notation

C_0 initial suspended sediment concentration, homogeneous over water depth.
C_s depth-averaged saturation concentration.
c suspended sediment concentration by mass.
c_{gel} gelling concentration.
c_s local saturation concentration.

e void ratio.
e_b efficiency factor in Bagnold's formula.
e_s efficiency factor in Bagnold's formula.
g acceleration of gravity.
h water depth.
h_s sedimentation depth.
K_s coefficient in scaling law for saturation.
k coefficient in Bagnold's formula.
k_s Nikuradse's roughness height.
n porosity.
Ri_f flux Richardson number.
$Ri_{f,cr}$ critical flux Richardson number.
t time.
U depth-averaged horizontal flow velocity.
u horizontal flow velocity.
u_* shear velocity.
W_s constant or characteristic settling velocity.
w_s effective settling velocity.
z vertical coordinate.
z_0 roughness height.
β Rouse parameter.
Γ_z eddy diffusivity.
Δ relative sediment density: $\Delta \equiv (\rho_s - \rho_w)/\rho_w$.
Δt time step in 1DV POINT MODEL.
κ von Kármàn constant.
ν kinematic viscosity.
ν_z eddy viscosity.
ρ bulk density of water-sediment suspension.
ρ_s density of primary sediment particles.
ρ_w density of water.
σ_T Prandtl-Schmidt number relating eddy diffusivity and eddy viscosity.
τ_b bed shear stress.
ϕ volumetric sediment concentration.

[48] **Acknowledgments.** I am very grateful to Massimo Cellino for making available the detailed data of his flume experiments. I also would like to thank Jurjen Battjes for his comments on the draft manuscript and two anonymous reviewers for their constructive critique. This work was carried out partly within the project "Predictive modeling of sediment transport and morphology in the Lower Yellow River" within the framework of the Strategic Alliance between China and Netherlands.

References

Bagnold, R. A. (1966), An approach to the sediment transport problem from general physics, *Geol. Surv. Prof. Pap.*, *422–I*.
Barr, D. I. H. (1967), Densimetric exchange flow in rectangular channels, *Houille Blanche*, *6*, 619–628.
Bastin, A., A. Caillot, and B. Malherbe (1984), Sediment transport measurements on and off the Belgium coast by means of tracers, paper presented at 8th International Harbour Congress, KVIV, R. Flemish Soc. of Eng., Antwerp, Belgium.
Cellino, M., and W. H. Graf (1999), Sediment-laden flow in open channels under non-capacity and capacity conditions, *J. Hydraul. Eng.*, *125*, 456–462.
Chien, N., and Z.-H. Wan (1999), *Mechanics of Sediment Transport*, translated from the Chinese by J. S. McNown, 913 pp., Am. Soc. Civ. Eng., Reston, Va.
Coleman, N. L. (1981), Velocity profiles with suspended sediment, *J. Hydraul. Res.*, *19*, 211–229.
Coleman, N. L. (1986), Effects of suspended sediment on the open-channel velocity distribution, *Water Resour. Res.*, *22*, 1377–1384.
Graf, W. H. (1977), *Hydraulics of Sediment Transport*, McGraw-Hill, New York.
Graf, W. H., and M. Cellino (2002), Suspensions in open channels; experimental study, *J. Hydraul. Res.*, *40*, 435–447.
Lesser, G. R., J. A. Roelvink, J. A. T. M. van Kester, and G. S. Stelling (2004), Development of a three-dimensional morphological model, *Coastal Eng.*, *51*, 883–915.
Liu, L., Z. Yang, and Z. Sheng (2003), Estimation of water renewal times for the middle and lower sections of the Yellow River, *Hydrol. Proc.*, *17*, 1941–1950.
Muste, M., and V. C. Patel (1997), Velocity profiles for particles and liquid in open-channel flow with suspended sediment, *J. Hydraul. Eng.*, *123*, 742–751.
Nezu, I., and R. Azuma (2004), Turbulence characteristics and interaction between particles and fluid in particle-laden open channel flows, *J. Hydraul. Eng.*, *130*, 988–1001.
Nielsen, P., and I. A. Teakle (2004), Turbulent diffusion of momentum and suspended particles: A finite-mixing-length theory, *Phys. Fluids*, *16*, 2342–2348.
Raudkivi, A. J. (1976), *Loose Boundary Hydraulics*, Pergamon, New York.
Richardson, J. F., and W. N. Zaki (1954), Sedimentation and fluidization, part I, *Trans. Inst. Chem. Eng.*, *32*, 35–53.
Royal Navy (1986), *Current Atlas of the Western Scheldt* (in Dutch), Hydrogr. Serv., The Hague, Netherlands.
Trowbridge, J. H., and G. C. Kineke (1994), Structure and dynamics of fluid muds on the Amazon continental shelf, *J. Geophys. Res.*, *99*, 865–874.
Turner, J. S. (1973), *Buoyancy Effects in Fluids*, Cambridge Univ. Press, New York.
Uittenbogaard, R. E. (1995a), The importance of internal waves for mixing in a stratified estuarine tidal flow, Ph.D. thesis, Delft Univ. of Technol, Delft, Netherlands.
Uittenbogaard, R. E. (1995b), Observations and analysis of random internal waves and the state of turbulence, paper presented at IUTAM Symposium on Physical Limnology, Int. Union of Theor. and Appl. Math., Broome, West. Aust, Australia.
Vanoni, V. A. (1946), Transportation of suspended sediment by water, *Trans. Am. Soc. Civ. Eng.*, *111*, 67–133.
Van Rijn, L. C. (1994), Principles of Sediment Transport in Rivers, Estuaries and Coastal Seas, Aqua, Oldemarkt, Netherlands.
Verlaan, P. A. J., and R. Spanhoff (2000), Massive sedimentation events at the mouth of the Rotterdam Waterway, *J. Coastal Res.*, *16*, 458–469.
Wan, Z. H., and Z. Y. Wang (1994), *Hyperconcentrated Flow*, *IAHR Monogr. Ser.*, 320 pp., A. A. Balkema, Brookfield, Vt.
Wang, G., and M. Xu (1999), Analysis of particularities pf 92.8 flood event in the Lower Yellow River, *Int. J. Sediment Res.*, *14*, 205–213.
Winterwerp, J. C. (2001), Stratification effects by cohesive and non-cohesive sediment, *J. Geophys. Res.*, *106*, 22,559–22,574.
Winterwerp, J. C. (2002), Scaling parameters for high-concentration mud suspensions in tidal flows, in *Proceedings in Marine Science*, vol. 5, edited by J. C. Winterwerp and C. Kranenburg, pp. 171–186, Elsevier, New York.
Winterwerp, J. C., and T. van Kessel (2003), Sediment transport by sediment-induced density currents, *Ocean Dyn.*, *53*, 186–197.
Winterwerp, J. C., and W. G. M. van Kesteren (2004), *Introduction to the Physics of Cohesive Sediment in the Marine Environment*, *Dev. Sedimentol.*, vol. 56, Elsevier, New York.
Winterwerp, J. C., W. T. Bakker, D. R. Mastbergen, and H. van Rossem (1992), Hyper-concentrated sand-water mixture flows over erodible bed, *J. Hydraul. Eng.*, *118*, 1508–1525.
Xu, J. (1999a), Erosion caused by hyperconcentrated flow on the Loess Plateau of China, *Catena*, *36*, 1–19.
Xu, J. (1999b), Grain-size characteristics of suspended sediment in the Yellow River, China, *Catena*, *38*, 243–263.
Xu, J. (2003), Sedimentation rates in the Lower Yellow River over the past 2300 years as influenced by by human activities and climate change, *Hydrol. Proc.*, *17*, 3359–3371.

J. C. Winterwerp, WL|Delft Hydraulics, P.O. Box 177, N-2600MH Delft, Netherlands. (han.winterwerp@wldelft.nl)